SUPPLEMENT TO THE *WELDING JOURNAL*, FEBRUARY 2009
Sponsored by the American Welding Society and the Welding Research Council

Hyperbaric GMA Welding of Duplex Stainless Steel at 12 and 35 Bar

Underwater welds show excellent mechanical properties when made under dry hyperbaric conditions

BY O. M. AKSELSEN, H. FOSTERVOLL, AND C. H. AHLEN

ABSTRACT

ABSTRACT. The present work was conducted to assess the weldability of duplex stainless steel under hyperbaric conditions relevant for future remote-controlled hot tap welding. This was achieved by horizontal welding with Inconel® 625 wire in V-grooves on plates in 2205 duplex steel in chamber pressures of 12 and 35 bar. The highest maximum hardness occurred in the heat-affected zone (HAZ) of the root bead, where HV_{10} values in the range from 260 to slightly above 280 were measured. The results showed that there is weld metal undermatch with respect to the yield strength (~ 460–490 MPa) , while the tensile strength (~ 740 MPa) was at the same level as that of the base plate. The notch toughness at –30°C was excellent for all positions tested (weld metal, weld interface, and weld interface +2 mm), and is far beyond current offshore requirements. The HAZ and weld metal were also characterized with respect to their microstructures. Although the welds were quite similar, the 35 bar weld appeared to have a thin zone (0–40 µm thickness) of ferrite in the HAZ close to the weld interface. The weld metal microstructure consisted of primary and secondary dendrite arms, which are the first to solidify. During this part of the solidification, solute elements are enriched in the liquid. With falling temperature, the solubility is probably exceeded with subsequent formation of intermetallic phases, as well as nitrides/carbides. Finally, the base metal dilution was subjected to microprobe analysis, showing large variations in weld metal chemical composition between different passes. The implications of the results with respect to corrosion and fracture toughness are discussed.

Introduction

Hot-tapping is now a well-established technology both onshore and offshore subsea in connection of branch pipelines to production pipeline systems without stopping production. The majority of the onshore hot taps is based on welding the branch pipe to the pipeline with subsequent tapping by using hydraulic drilling. So far, the subsea hot taps have been made by divers using welded branch pipe connections, preinstalled hot tap tees, or by using retrofitted hot tap clamps with elastomer seals between the clamp and the main pipe. However, elastomer seals used as a single barrier are often regarded as a risk with reduced reliability and safety. The reason is that the elastomer can deteriorate mainly due to swelling in hydrocarbon service with a subsequent extrusion in the gap between the clamp and the main pipe. To use welded seals is regarded as a method to improve the lifetime, reliability, and safety. So far, less than ten hot-taps have been carried out on subsea pipelines in the North Sea. These hot-taps have provided very cost-effective solutions, but are based on an approach using divers and it is thus limited to water depths where diving may be applied. On the Norwegian continental shelf this limitation is 180 m maximum. Accordingly, there is a need for diverless and fully remote-controlled technology for future hot tapping. This new remote system will also represent a substantial cost reduction since the offshore vessel alone used for the remote equipment is approximately half the daily cost of an offshore vessel with diver support, without including the additional cost of diver qualification (Ref. 1).

KEYWORDS

Hyperbaric Welding
Gas Metal Arc Welding
GMAW
Duplex Stainless Steel
Inconel® 625 Weld Metal
Mechanical Properties
Microstructures

The fully remote hot tapping will be done using gas metal arc welding (GMAW), which represents a new situation in the Norwegian oil and gas industry. Up to now, all diver-assisted remotely controlled welding has been done by gas tungsten arc welding (GTAW) through the Pipeline Repair System (PRS) pool. Here, the research and development leading to this technology were launched in the middle of the 1970s (Refs. 2–7), with studies on how the weld metal chemical composition and moisture pickup were affected by pressure (water depth) in welding of low-alloy steels. More recently, the effects of hydrogen and oxygen have also been evaluated for higher-alloyed steels, such as duplex stainless steels (Ref. 8) and supermartensitic 13% Cr stainless steels (Ref. 9). However, since the remotely controlled GTAW has been developed for industrial use offshore in pipeline tie-ins and repair, the development of reliable equipment (Refs. 10–12) has been a major issue. All this is now available under the PRS pool, and has been overviewed in a recent paper (Ref. 13), showing that more than 70 offshore pipeline tie-ins have been completed so far.

Hyperbaric GMA welding has been developed over the past decades at Cranfield University, and is fully demonstrated for orbital V-groove welding (Refs. 14, 15) with successful process operation at up to 2500-m water depth. It has already been selected as the process method for a sleeve repair technique for pipelines for operation at up to 1000 m in

O. M. AKSELSEN and H. FOSTERVOLL are with SINTEF, Trondheim, Norway. C. H. AHLEN is with StatoilHydro Research Center, Trondheim, Norway.

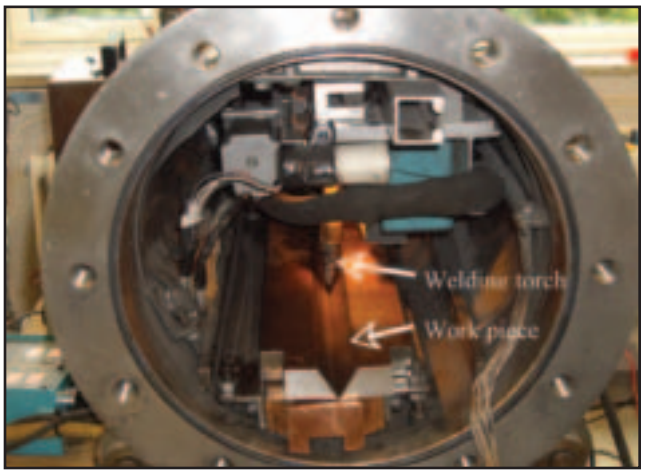

Fig. 1 — Hyperbaric welding chamber.

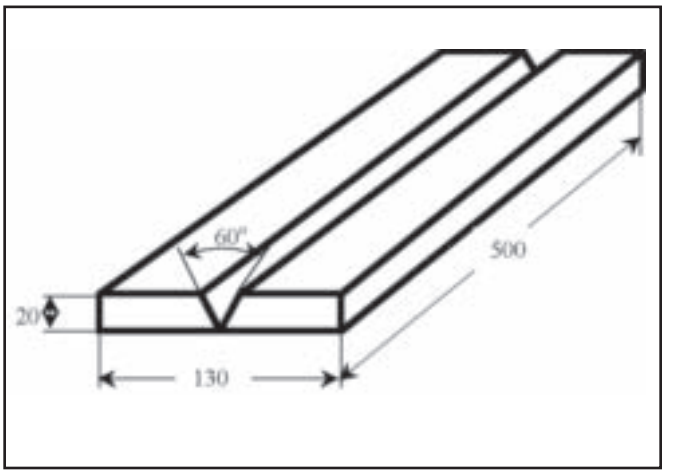

Fig. 2 — Dimensions of workpiece (in mm).

the first instance. More information about equipment, including details on the structural design and installation of the hot tap tee can be found elsewhere (Ref. 16). However, the present investigation is part of the development of robust GMA welding technology to be used in future diverless, remote-controlled tie-in and hot tap welding. Welding tests were carried out in a small chamber pressurized to 12 and 35 bar, corresponding to 110- and 340-m water depth. A conventional (22% Cr, 5% Ni) duplex stainless steel was selected as plate material since it may be an alternative for hot tap branch pipes. It was intended to identify a robust welding wire which gives excellent resistance against corrosion and hydrogen-induced cracking, and a strength level similar to that of the base metal. For this purpose, a solid Inconel® 625 Ni-based superalloy wire was selected. It was shown that excellent mechanical properties are achievable.

Materials and Experimental Procedure

Materials

The chemical compositions of the base metal and the welding wire are outlined in Table 1. The base metal is a 20-mm-thick plate of classical 2205 duplex stainless steel (UNS S31803, 22% Cr-5% Ni) with 3% Mo and 0.18% N. Its room-temperature yield and tensile strengths are 518 and 744 MPa, respectively. The selected wire is Inconel® 625, which is a nickel-based (~66%) superalloy supplied with 0.9 mm diameter. The major alloying elements are Cr (~21%), Mo (~9%), Nb (3.3%), and Fe (~1%).

Welding

Welding tests at 12 bar (Weld 1) and 35 bar (Weld 2) were carried out in a cylindrical chamber with volume of 100 L and internal diameter of 350 mm — Fig.1. The chamber was equipped with a conventional wire feeder and GMA welding gun rigged up for V-groove welding of plates in the flat position. The length of the workpieces were 500 mm with total width of 130 mm and thickness of 20 mm. A 60-deg V-groove was machined for welding — Fig.2. The power source comprised three modified Fronius Transpocket TP450s in series. The chamber was pressurized with 99.996% pure argon, and no separate shielding gas through the welding gun was used. Prior to pressurizing, the chamber was evacuated to 0.1 bar. The oxygen content in the chamber was below 200 ppm when the welding started. The welding parameters used for both welds are shown in Table 2. The interpass temperature was maximum 50°C. Welding was done without stiffeners, and the plates were thus free to deform. As expected, substantial angular distortion was found.

Chemical Analysis

Samples were cut for full chemical analysis for both Welds 1 and 2. These were taken in the weld center (mid thickness). Sulfur and carbon were analyzed by infrared combustion, while oxygen and nitrogen contents were found by inert gas fusion analysis. An optical emission spectrometer was used to determine the content of all other elements.

Mechanical Testing

Mechanical testing included both all-weld-metal tensile testing and Charpy V-notch toughness testing at –30°C, and was carried out in agreement with the DnV offshore standard (Ref. 17). Tensile bars were cut from the weld metal with length axis parallel to the welding direction. The specimens were 48 mm long with a 24-mm gauge length of 4-mm diameter, while the 12-mm-long sample heads were M8 threads. Two parallels were included. Charpy V samples of 10- × 10-mm cross sections and 55-mm lengths were cut transverse to the welding direction. These were taken out from the welds at a distance of 2 mm below the plate surface. The notch was positioned to provide fracture along the welding direction. A total number of 3 parallels were tested at –30°C. Three different notch positions were included, i.e., the weld metal center, the weld interface, and the weld interface + 2 mm. These are shown schematically in Fig. 3. For all positions, macro-etching was done to locate the notch. For the weld interface position, the intention was to achieve roughly 50% weld metal and 50% HAZ along the notch.

Metallography

One macro specimen was cut as cross

Table 1 — Chemical Composition of Wires and Base Material (elements in wt-%)

Material	C	Si	Mn	P	S	Cr	Ni	Mo	Al	Ti	N
2205 duplex steel	0.016	0.4	1.4	0.023	0.001	22.3	5.7	3.1	—	—	0.18
Inconel 625 wire[a]	0.015	<0.05	0.03	<0.005	0.0006	20.68	65.74	8.81	0.24	0.063	-

(a) With 3.23% Nb, <0.05% Co, 1.09% Fe.

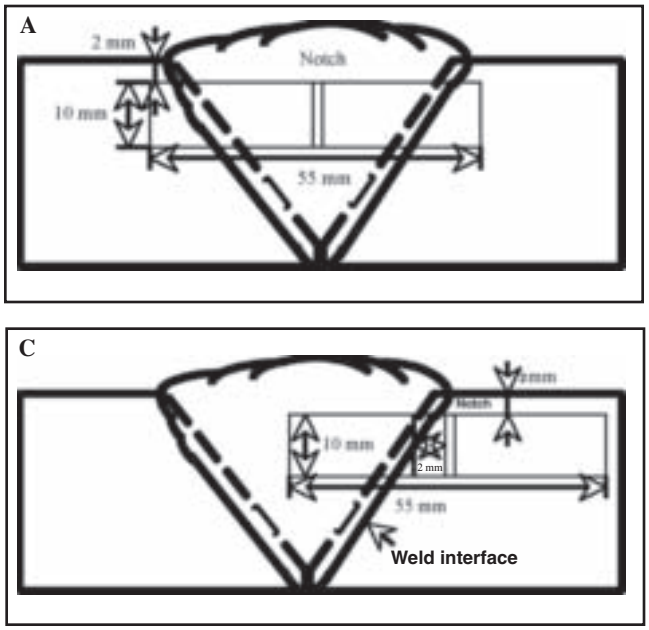

Fig. 3 — Schematic illustration of Charpy V-notch location. A — Weld metal center; B — weld interface; C — weld interface + 2 mm.

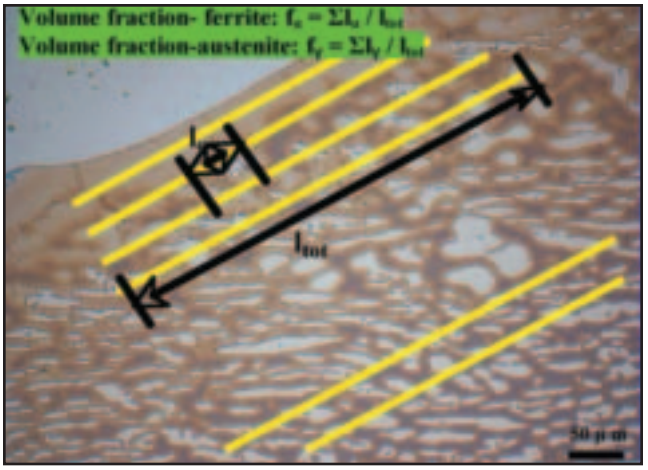

Fig. 4 — Schematic illustration of measurements (rough estimates) of ferrite volume fractions in the HAZ.

sections from each plate weld and prepared using standard metallographic techniques. Vickers hardness traverses with 10-kg load (HV_{10}) were run across the entire weld and the base metals both in the cap and root positions. After macro photos were taken, the specimens were examined in more detail for microstructure characterization. For HAZ examination, the specimens were etched in NaOH solution. The austenite-ferrite contents were estimated based on the mean linear interception length concept, as briefly defined in Ref. 18. This was done on micrographs taken at a magnification of 200×, and is schematically illustrated in Fig. 4. Subsequently, the Inconel 625 weld metal was examined based on electrolytical etching of specimens in 10% oxalic acid (aqueous solution) for 20–30 s, operating at room temperature with 6 V and 1 A.

Results and Discussion

Weld Defects

Both Welds 1 and 2 were completed with 14 individual stringer beads. Due to the one-sided welding without the use of stiffeners, substantial angular distortion took place. Thorough examination in unetched and etched macro specimens in an optical microscope did not reveal any critical weld defects.

Weld Metal Chemical Composition

The weld metal chemical composition is outlined in Table 3. It is seen that some Ni is "lost" due to pickup of iron through base metal dilution (6.7 wt-% Fe for both welds). The Ni content is slightly above 60 wt-%, while the Inconel wire had almost 66 wt-%. Molybdenum is also somewhat lower in the weld than in the wire. The nitrogen concentration was found to be 220–230 ppm, which is much lower than the level in the base metal (0.18 wt-% N). The weld metal oxygen content is low (120 ppm). The carbon content was also low (0.01 wt-%). Finally, there is a slight pickup of Mn due to base metal dilution, i.e., from 0.03 wt-% in the wire to 0.18–0.19 wt-% in the welds.

Hardness Profiles

Hardness traverses were performed on both the root and the cap side of the macro specimens. The maximum individual hardness values found in the base metal, HAZ, and weld metal are plotted in Fig. 5 and listed in Table 4, where minimum, maximum, and average values are summarized. The highest individual level was found in the HAZ of the root bead,

Table 2 — Welding Parameters

Parameter	12 bar (Weld No.1)	35 bar (Weld No. 2)
Welding current (average)	170 A	166 A
Arc voltage (average)	28.8 V	29.8 V
Welding speed	6 mm/s	
Wire feed rate	10 m/min	
Interpass	Maximum 50°C	

Table 3 — Weld Metal Chemical Composition (elements in wt-%)

Weld No.	C	Si	Mn	S	Cr	Ni	Mo	Nb	Fe	Al	Ti	N	O
1 (12 bar)[a]	0.01	<0.1	0.18	0.002	21.1	60.4	7.9	3.2	6.7	0.17	0.09	0.022	0.012
2 (35 bar)[a]	0.01	<0.1	0.19	0.002	20.9	60.8	7.7	3.2	6.7	0.17	0.09	0.023	0.012

(a) With 0.08% Cu.

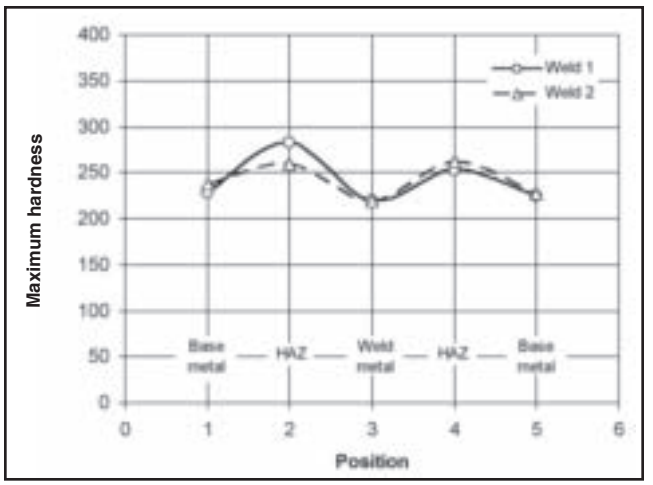

Fig. 5 — Hardness distribution in Welds 1 and 2.

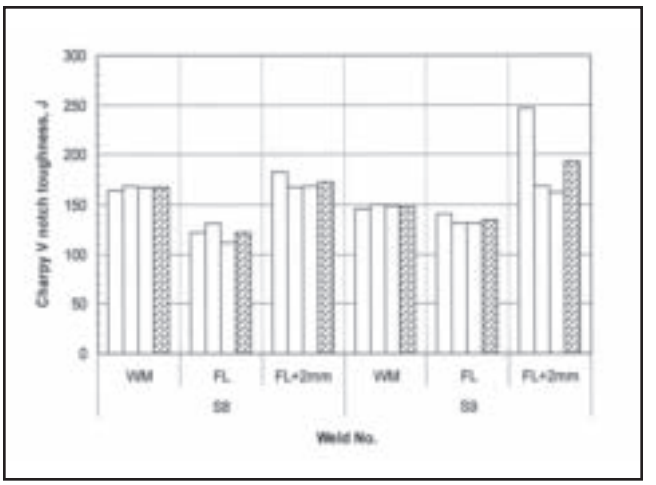

Fig. 6 — Charpy V-notch toughness at –30°C (open rectangles: individual values, filled rectangles: average value).

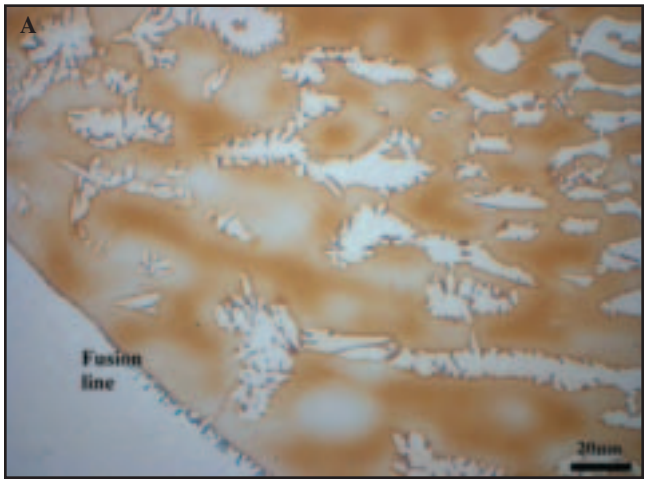

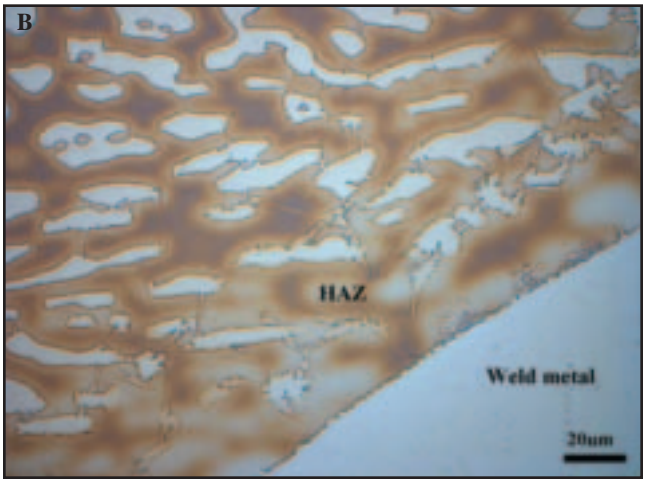

Fig. 7 — HAZ microstructure of cap bead. A — Weld 1; B — Weld 2.

Table 4 — Hardness Distribution in the Welds

Weld No.	Base Metal			HAZ			Weld Metal		
	Min	Max	Mean	Min	Max	Mean	Min	Max	Mean
S8	217	222	229 (12 indendations)	229	283	246 (17 indendations)	193	220	204 (6 indendations)
S9	214	225	238 (10 indendations)	239	284	249 (9 indendations)	201	220	208 (7 indendations)

Table 5 — Results from All Weld Metal Tensile Testing

Weld No.	Yield Strength $R_{p0,2}$, MPa	Tensile Strength R_m, MPa	Elongation at Fracture A_5, %	Yield to Tensile Ration R_{p02}/R_m
Base metal	518	744	—	0.70
1 (12 bar)	491	739	67	0.66
2 (35 bar)	468	735	70	0.64

i.e., 283–284 HV_{10} for both welds, both with average close to 250. The maximum weld metal hardness was relatively low, 220 HV_{10} with mean values of 204 and 208 for Welds 1 and 2, respectively. The base metal hardness varied between 220 and 240 HV_{10}. These hardness values are similar to previously reported results (Refs. 1, 19) using the Inconel wire in welding of low-alloy API X65 steels for a wide range in water depths (pressures between 12 and 100 bar).

Tensile Properties

The results from all-weld-metal tensile testing are summarized in Table 5. The average yield strengths were 491 and 468 MPa for Welds 1 and 2, respectively, with

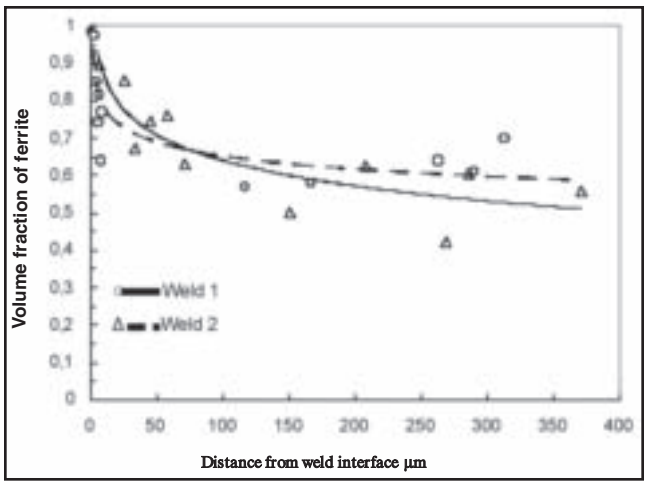

Fig. 8 — Variation in HAZ volume-fraction of ferrite as function of distance from the weld interface (the lines are "trend lines").

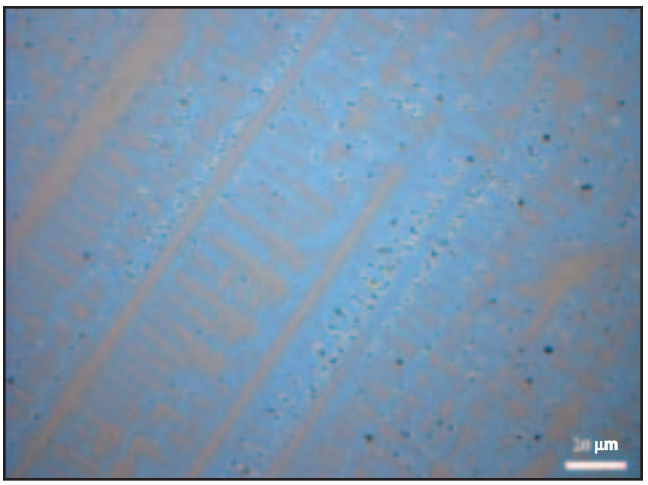

Fig. 9 — Microstructure in primary weld metal, Weld 1.

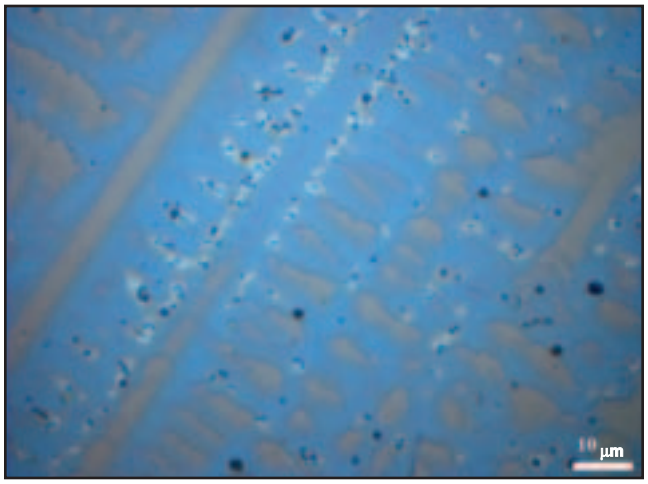

Fig. 10 — Close-up of area in Fig. 6, Weld 1.

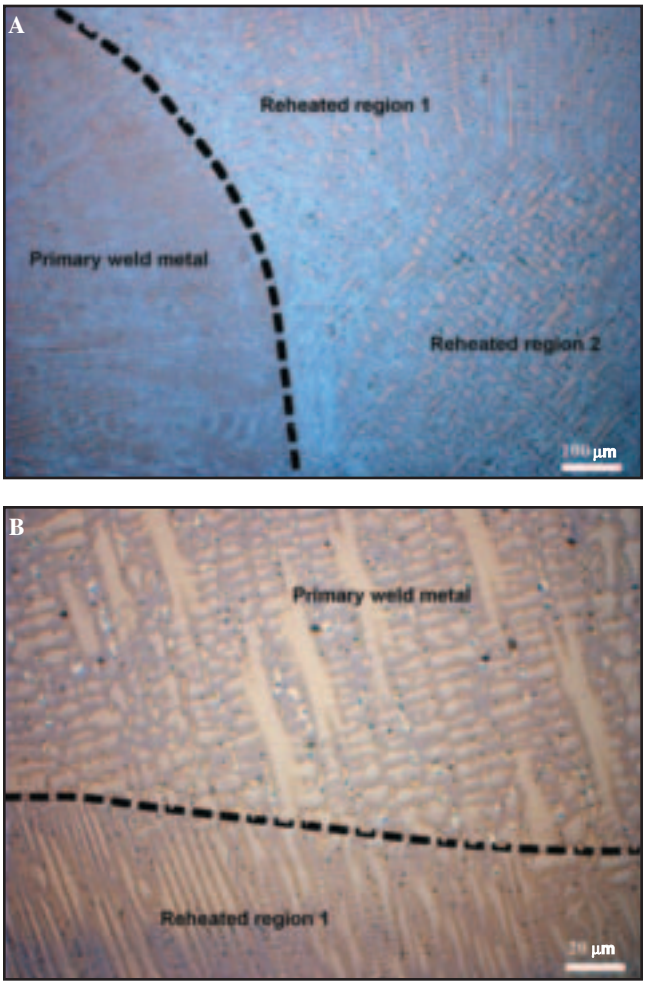

Fig. 11 — Overview of reheated weld metal. A — Weld 1; B — Weld 2.

corresponding tensile strengths of 739 and 735 MPa. This means that both welds represent an undermatch situation, i.e., weld metal yield strength is lower than that of the base metal (518 MPa). However, the yield strengths of both welds are higher than the minimum specified yield strength for the base metal, satisfying current requirements set to X65 pipe (65,000 lb/in^2 or 450 MPa in yield strength). The tensile strength is similar to that of the base metal.

Notch Toughness

The results from impact testing are illustrated in Fig. 6. Three positions were tested; 1) weld metal, 2) weld interface, and 3) weld interface + 2 mm. It is seen that all positions possessed excellent toughness (> 100 J) at –30°C. Moreover, the scatter is quite low between the different parallels. For Weld 1, the weld metal toughness exceeded 150 J, while Weld 2 had values slightly below 150 J. However, this toughness is still a bit lower than earlier reported values for X65 welds, where the Inconel 625 weld metal had toughness values beyond 200 J (Ref. 19). High toughness of Inconel 625 weld metals are expected since there is no transition temperature from ductile to brittle fracture for nickel alloys. The weld interface toughness was also very good with individual values in the range 112–132 and 132–141 J for Welds 1 and 2, respectively. Thus, the two welds are quite similar. In addition, the scatter in toughness is quite low in spite of the fact that the impact value represents a mixture between the duplex HAZ and the Inconel 625 weld metal. Moreover, the weld interface is expected to fluctuate along the weld, which may imply that the ratio between the HAZ and the weld metal distributed along the notch in the Charpy specimen will vary almost from 0 to 1.0. The Charpy specimens have not been examined after the completion of testing, so this ratio is not yet known. Therefore, it is difficult to assess the present results in a

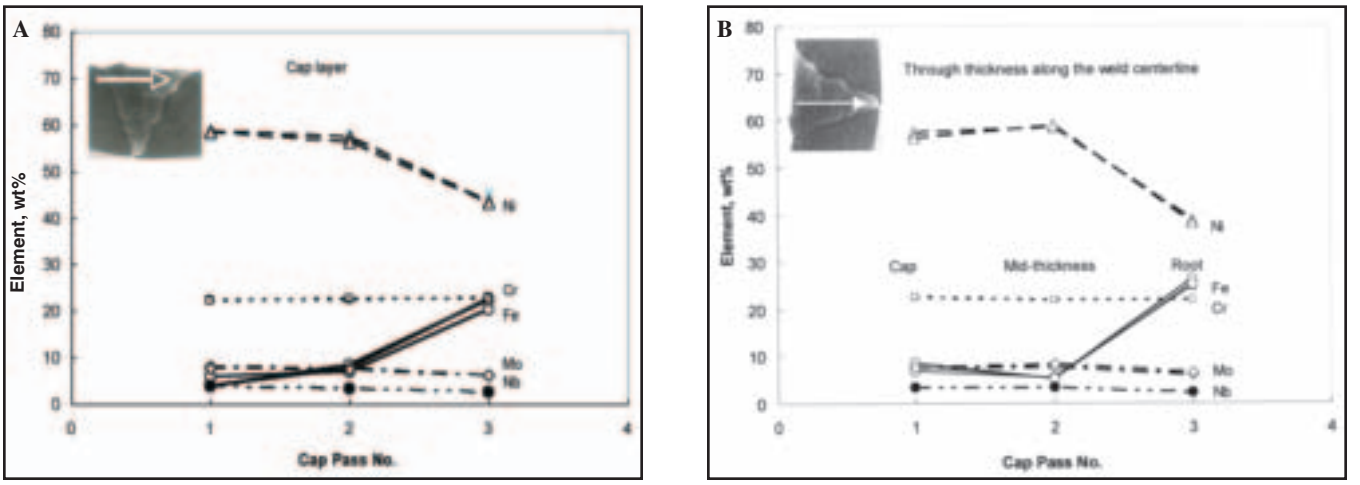

Fig. 12 — Variation in element concentration in Weld 2. A — Cap layer; B — through plate thickness.

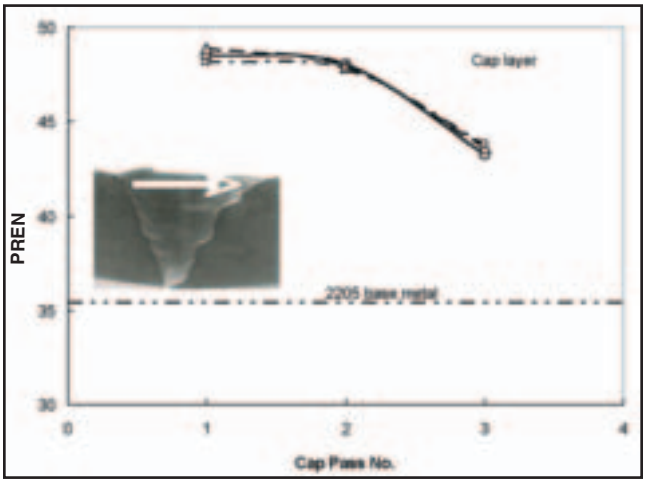

Fig. 13 — Pitting resistance equivalent (PREN) values across the cap layer of Weld 2. The nitrogen contents are 0.18% in the 2205 base metal, 220 ppm in Weld 1, and 230 ppm in Weld 2. The content in the Inconel 625 wire is not known.

statistical manner, but there is no reason to believe that the toughness should suddenly drop to levels below the minimum requirements set in current offshore specifications. For X65 type of quality, the Charpy requirements are minimum single and average values of 38 J and 45 J, respectively (Ref. 17). For an X70 pipe, the corresponding values are raised to 40 and 50 J. With these requirements in mind, the welds are clearly acceptable in terms of mechanical properties.

However, the impact values are much lower than that previously reported for weld interface notched specimens when welding low-alloy X65 steel with Inconel 625 wire (Ref. 19). On the other hand, the toughness level is beyond that reported in conventional (at 1 bar) flux cored arc and submerged arc welding, which was in the range of 63–76 and 100–141 for the weld interface and HAZ, respectively (quoted in Ref. 20). For the weld interface toughness, the welding consumables will obviously be very important, and the Inconel 625 appears to give satisfactory robustness.

Microstructure Examination

The HAZ microstructure of Weld 1 consists of ferrite and austenite (Fig. 7A), but with more ferrite than in the base metal. Weld 2 also had similar microstructure in the HAZ, but here there was found a 40–80 μm narrow layer at the weld interface with only ferrite — Fig.7B. This observation is probably linked to the welding arc restriction with increasing chamber pressure (water depth), as the case when going from weld deposition of Weld 1 at 12 bar to Weld 2 at 35 bar. The smaller arc area may thus, in turn, cause more rapid cooling, which may be sufficient to prevent austenite nucleation within a narrow band close to the weld interface. An additional cause may be diffusion of nitrogen from the HAZ to the weld metal due to the large concentration gradient in nitrogen, i.e., from 0.18% N in the base metal to 220–230 ppm in the weld metal. This diffusion may take place when the region close to the weld interface is brought up to the temperature of partially melting or when it is fully ferritic where the diffusion is more rapid than in austenite. An eventual verification of this phenomenon would be possible through more detailed microprobe analyses performing several line scans across the narrow ferrite band and the weld interface in both Welds 1 and 2 for comparison of the nitrogen distribution.

A high-volume fraction of ferrite in the high-temperature region of HAZ in duplex stainless steels is not surprising, but rather usual. This is due to the grain coarsening of the ferrite taking place during the heating cycle followed by rapid cooling, which together with the grain coarsening may prevent austenite formation. Such high amount of ferrite is considered detrimental to notch toughness and also the corrosion resistance through possible precipitation of chromium nitrides (Cr_2N or CrN) in the ferrite which may take place due to limited solubility of nitrogen in ferrite. The Cr nitrides will then reduce the PREN value of the matrix with a possible rise in the pitting corrosion susceptibility. In addition, an eventual diffusion of nitrogen into the weld metal due to the large concentration gradient may cause a further reduction of the local pitting corrosion resistance. Therefore, it is usual to specify a certain range in the ferrite content to satisfy offshore requirements in welding of duplex stainless steels. One example is discussed later in this paper.

The ferrite and austenite volume fractions were estimated using mean linear intercept technique to quantify the microstructure in different distances from the weld interface. It should be noticed that the distance from the weld interface is roughly approximated due its bowing nature. The results are shown in Fig. 8. This plot confirms the high-volume fraction of ferrite in the HAZ of both welds close to the weld interface, and that Weld 2 contains almost ferrite only in a narrow region, as already noticed in the micrograph in Fig. 7B. The statistics are quite poor here, and there is certainly also a large scatter. The results must therefore be treated with some care. It should be kept in mind that the DnV offshore standard prescribes the volume-fraction of

ferrite to be within the range from 0.35 to 0.55 for the base metal, and between 0.35 and 0.65 for the HAZ and the weld metal in welding of duplex stainless steel with matching consumables (Ref. 17). Therefore, a part of the HAZ in both welds, representing a distance from the weld interface of 60 μm is clearly outside the specified range. In a welding procedure qualification situation, this fact would have to be dealt with through verification of sufficient mechanical and corrosion properties through testing.

The weld metal microstructure of Weld 1 is shown in Fig. 9 and reveals dendrite solidification. Similar features were found in the study of Weld 2 microstructures. The primary dendrite arms (gray-brown) solidify first, followed by secondary dendrite arms, and finally, the interdendritic regions (blue) where enrichment in solute elements takes place, primarily Nb and Mo. With falling temperature during cooling, the solubility of these solutes decreases with subsequent formation of intermetallic phases and precipitation of particles. This point is shown in Fig. 10, where particles are entirely present in the interdendritic regions, further underlining the microscopic segregation of solutes. These particles may be carbides (e.g., NbC, black spots in the figures) or intermetallic particles (e.g., Laves phase, blue particles in the figures). Due to the thermodynamics with mutual full solid solubility between Nb and Mo, and between Cr and Mo, there are several possible stoichiometries of the intermetallic phases. In the Ni-Nb binary system, Ni_8Nb and Ni_3Nb may form on the Ni-rich side. For binary Cr-Nb mixture, the Cr_2Nb may exist. In binary Ni-Mo alloys, several phases are possible, both stable and metastable phases may form. Previous microprobe analyses of similar Inconel 625 weld metals (Ref. 19) have confirmed the presence of Nb-rich particles present, often with Ti, N, O, and C, indicating that the analysis volume comprises of NbN (or NbCN), together with Ti-containing nonmetallic inclusions. The intermetallic particles seemed to be consistent with a $(Me1)_2(Me2)$ kind of phase, suggesting them to be Laves phase of the form $(Ni,Cr,Fe)_2(Nb,Mo)$. Nb and Mo have large atomic radii, while Ni, Cr, and Fe have smaller, but similar-sized radii. Due to their presence, questions can be raised concerning their effects on mechanical properties and corrosion resistance. However, intermetallic precipitates represent the major strengthening mechanism in higher-alloyed Ni-based superalloys like Inconel 718.

The reheated weld metal microstructure is shown in Fig. 11. Due to the absence of solid-state phase transformations, the microstructure of the reheated region is very similar to that of the primary weld metal. Still, redistribution of alloying elements may take place, depending on the temperature and time available for diffusion.

Base Metal Dilution

Base metal dilution may change the chemical composition locally, and may thus be important to corrosion resistance and local fracture toughness. Such dilution was examined in different beads and in the HAZ to obtain information on the local variations in chemical composition. The chemical analyses were performed with JEOL JXA-8500F instrument equipped with a wavelength dispersive spectrometer (WDS). Three individual analyses were performed per location, and large variations were found for certain beads. The results are plotted in Fig. 12 in terms of element concentration (wt-%) for Fe, Ni, Cr, Mo, and Nb. For the cap layer data plotted in Fig. 12A, is it seen that the base metal dilution is fairly high for sidewall beads, with more than 20 wt-% Fe in one of these beads. Here, the Ni content was reduced from about 66 wt-% in the welding wire to approximately 44 wt-%, which confirms a base metal dilution of about 20%. The Cr content in the weld metals (22–23 wt-%) were similar as their origins, namely the welding wire and the base metal. The Mo and Nb concentrations are slightly lower in the cap layer than in the wire due to base metal dilution. In the central bead of the cap layer, there is as expected much lower base metal dilution with 7–9 wt-% Fe, indicating a dilution of 6–8%. As expected, the vertical (through thickness) element distribution plotted in Fig. 12B demonstrates that the highest base metal dilution is found in the root pass. Here, the Fe concentration is about 26 wt-%, with Ni content of 56–58 wt-%. By contrast, the mid-thickness central weld pass revealed low dilution with 5–6 wt-% Fe and 58–59 wt-% Ni. As with the horizontal cap layer analyses, the Cr, Mo, and Nb contents were fairly constant throughout the plate thickness along the weld centerline. The vertical analyses along the sidewall of the groove showed large scatter in the Ni content, i.e., 41–55 and 39–58 wt-% for Welds 1 and 2, respectively. These variations are also associated with similar variation in the Fe content, which is due to pertinent variations in positioning (welding gun) of the individual stringer beads in the groove.

It should be noticed that the volume of analysis is only in the order of 1 μm^3, by contrast to the large volume involved in base metal and weld metal chemical analyses (typically 1 in. in diameter). Microprobe analysis may detect eventual macro/micro segregations, and the potent differences in composition between ferrite and austenite. This may explain the small deviations between the data in Fig. 12 for the base metal and the chemical composition data in Tables 1 (base metal) and 3 (weld metal).

Practical Implications

The quantitative effects of the variations in chemical composition and base metal dilution are not possible to assess from the present investigation. There are numerous corrosion types that may take place, including general corrosion, pitting corrosion, crevice corrosion, stress corrosion cracking, sulfide stress corrosion cracking, intergranular corrosion, galvanic corrosion, contact corrosion, and the subject in focus over the past decade, hydrogen-induced cracking (HIC).

Under certain conditions, particularly involving high concentrations of chlorides (such as sodium chloride in seawater), moderately high temperatures and exacerbated by low pH (i.e., acidic conditions), very localized corrosion can occur leading to perforation of pipes and fittings, etc. Grades high in chromium, and particularly molybdenum and nitrogen, are more resistant to pitting corrosion. The Pitting Resistance Equivalent Number (PREN) has been found to give a good indication of the pitting resistance of stainless steels. The PREN can be calculated as (in wt-%):

$$PREN = Cr + 3.3\,Mo + 16\,N$$

The PREN values for the base metal and the weld metal are 35.4 and 50.1, respectively. Since the weld metal represents a mixture between these two extremes, the PREN would be expected to fall between them. This is further evidenced by the plots in Fig. 13 illustrating the PREN value distribution in the cap layer of Weld 2. Similar results were found for Weld 1. Therefore, the welds should have sufficient resistance to pitting with all PREN values above 43. However, as previously noticed, high ferrite content in the HAZ may cause precipitation of Cr nitrides, which again may change the resistance against localized corrosion attacks.

Hydrogen-induced cracking may take place under cathodic protection where the potential provides hydrogen generation. Hydrogen atoms may enter the material with subsequent degradation of material toughness as a consequence. Alternatively, hydrogen may enter the material by a corrosion process by sour service (sulfide stress corrosion cracking). In order to resist sour service, a maximum hardness level of 22 Rockwell C (= 248 Vickers hardness) is required (Ref.

21). However, this is valid for carbon steel only. For wrought and cast duplex stainless steels in the solution-annealed and liquid-quenched condition, hardness requirement is set to 28 HRC (= 286 HV) maximum (Ref. 21). Heat treatments to increase strength or hardness are not allowed. For welds in duplex stainless steels (Ref. 22), the hardness may not exceed an average value of 310 HV_{10}, and no individual reading may exceed 320 HV_{10}. In addition, the measured weld metal and HAZ ferrite volume fraction must be between 0.35 and 0.65 (Ref. 17). In the present investigation, the highest HV value in the HAZ was found to be 283 in the HAZ of the root pass in Weld 1. It should therefore satisfy current requirements set to maximum hardness. The same is the case for Weld 2, but here the ferrite volume fraction is almost 1.0 in a narrow region (0–40 µm thickness) at the weld interface. The implication of this finding is not clear since all toughness values were very high, including those of the weld interface. However, it may influence the resistance against localized corrosion attacks such as pitting. Such testing was outside the scope of the present investigation.

Conclusions

The present work was carried out as part of the development of hyperbaric gas metal arc (GMA) welding for future remote-controlled hot tap welding. The welding trials for mechanical testing and metallographic inspection were performed at 12 and 35 bar with 2205 duplex stainless steel base metal and Inconel 625 solid wire. The following main conclusions can be drawn:

- The highest single hardness value was 283 HV_{10}, found in the HAZ of the 2205 duplex steel. All other values were below about 250. However, it should be noticed that these welds were allowed to freely distort since no stiffeners were used.
- Both welds represent a strength undermatch situation where weld metal yield strength is lower than that of the base metal (518 MPa). The yield strengths were 491 and 468 MPa for Welds 1 and 2, respectively, with corresponding tensile strengths of 739 and 735 MPa. The tensile strength is similar to that of the base metal.
- Three positions were tested with respect to notch toughness; 1) weld metal, 2) weld interface, and 3) weld interface + 2 mm. As shown, all positions possessed excellent toughness (> 100 J) at –30°C.
- Some concern may be raised with respect to the high ferrite volume fraction (~ 1.0) in a narrow (up to 40 µm) region at the weld interface, although the implication of this finding is not clear since all toughness values were very high, including those of the weld interface.
- The weld metal microstructure study revealed dendrite solidification with primary and secondary dendrite arms, and interdendritic regions with enrichment in solute elements, primarily Nb and Mo. The decreasing solubility of these solutes during cooling resulted in formation of intermetallic phases. Along with this, precipitation of particles took place.
- Base metal dilution resulted in large local variations in the weld metal chemical composition. The quantitative effects of these variations in chemical composition cannot be assessed from the present investigation, but the low hardness level should satisfy requirements set for sour (or at least mildly sour) service.

Acknowledgments

The authors wish to thank StatoilHydro and Gassco for financial support. The assistance by Morten P. Raanes (microprobe analyses) and Synnøve Åldstedt (metallography) is gratefully acknowledged.

References

1. Woodward, N. J., Fostervoll, H., Akselsen, O. M., Ahlen, C. H., Berge, J. O., and Armstrong. M. 2007. Evaluation of welding procedures and consumables for hyperbaric GMAW for diverless retrofit tee hot tap applications. *17th Int. Offshore and Polar Eng Conf.* (ISOPE), Lisbon, Portugal.

2. Grong, Ø., Olson, D. L., and Christensen, N. 1985. *Metal Constr.* 17, 810R–814R.

3. Christensen, N. 1983. The metallurgy in underwater welding. *Proc. Int. Inst. Weld. Conf. Underwater Welding*, Trondheim, Norway, pp. 71–79, Pergamon Press.

4. Kvaale, P. E., Gjermundsen, K., and Christensen, N. 1983. Moisture absorption of basic electrodes under pressure up to 33 bar. *Proc. Int. Inst. Weld. Conf. Underwater Welding*, Trondheim, Norway, , Pergamon Press.

5. Knagenhjelm, H. O., Gjermundsen, K., Kvaale, P. E., and Gibson, D. 1982. Hyperbaric TIG welding to 500 m simulated depth. *Proc. Int. Conf. Underwater Technology* (OTC), Bergen, Norway.

6. Christensen, N., and Gjermundsen, K. 1977. Effects of pressure on weld metal chemistry. Int. Inst. Weld. Document IIW-doc. 212-395-77.

7. Christensen, N., and Gjermundsen, K. 1976. Effects of pressure on weld metal chemistry. Int. Inst. Weld. Document IIW-doc. 212-384-76.

8. Håbrekke, T., Kvaale, P. E., and Rørvik, G. 1996: Hyperbaric welding of duplex stainless steels. *Proc. Int. Conf. Offshore Mechanics and Arctic Engineering* (OMAE), Firenze, Italy.

9. Aune, R., Knagenhjelm, H. O., and Hårsvær A. 2005. Hydrogen and oxygen pick-up in hyperbaric TIG welding of supermartensitic 13% Cr stainless steel with matching filler wire. *Proc. 24th Int. Conf. on Offshore Mechanics and Arctic Engineering* (OMAE), Paper No. OMAE2005-67554, Halkidiki, Greece.

10. Håbrekke, T., and Knagenhjelm, H. O. 1989. Hyperbaric mechanized TIG welding for underwater tie-in and repair operations, using the IMT (Integrated Modular Tool) system. *Proc. Int. Conf. on Welding under Extreme Conditions,* Int. Inst. Weld., Helsinki, Chap. V, pp. 247–260.

11. Berge, J. O., Håbrekke, T., and Knagenhjelm, H. O. 1991. Automation in underwater hyperbaric pipeline welding. *Proc. 10th Int. Conf. on Offshore Mechanics and Arctic Engineering* (OMAE), Stavanger, Norway, Vol. 111-A, pp. 163–167.

12. Håbrekke, T., Armstrong, M., and Berge, J. O. 1997. Deep water pipeline welding and repairs using modern computer technology to create a diverless future for Statoil. *Proc. 7th Int. Conf. on Computer Technology in Welding,* San Francisco, NIST Special Publication 923, pp. 31–41.

13. Akselsen, O. M., Aune, R., Fostervoll, H. and Hårsvær, A. H. 2006. Dry hyperbaric welding of subsea pipelines, *Welding Journal*, Vol. 85(6): 52–55.

14. Richardson, I. M., Woodward, N. J., and Billingham, J. 2002. Deepwater welding for installation and repair — A viable technology?. *12th Int Conf on Offshore and Polar Engineering* (ISOPE), Kita-Kyushu, Japan.

15. Richardson, I. M., Woodward, N. J., and Billingham, J. 2002. Diverless underwater GMA welding, IIW-Doc. SCUW-197-02, *Proc 55th Annual Assembly of the International Institute of Welding* (IIW), IIW Selected Committee for Underwater Welding (SCUW), Copenhagen, Denmark, pp. 1–19, IIW.

16. Apeland, K. E., Berge, J. O., Verley, R., Woodward, N. J., and Armstrong, M. 2004. Deep water remote welding technology for pipeline repair and hot-tapping. *Proc Int. Conf. & Ex. on Deep Offshore Technology* (DOT), Houston, Tex.

17. DnV (2007), Det norske Veritas Offshore Specification DNV-OS-F101: *Submarine Pipeline Systems*.

18. ASTM Standard. 1996. Designation: E 112-96, *Standard Test Methods for Determining Average Grain Size*.

19. Akselsen, O. M., Fostervoll, H., and Ahlen, C. H. 2008. Hyperbaric gas metal arc welding of API X65 pipeline steel at 12, 25, and 35 Bar. *18th Int Offshore and Polar Eng Conf.*, (ISOPE) Vancouver, Canada.

20. Nowacki, J. 2004. Duplex steel welding problems in the building of cargo ships, *Weld. Int.,* Vol. 18, pp. 509–515.

21. NACE Standard MR0175-2003: *Sulfide Stress Cracking Resistant MetallicMaterials for Oilfield Equipment*. Houston, Tex.

22. NACE Standard MR0103-2003, *Materials Resistant to Sulfide Stress Cracking in Corrosive Petroleum Refining Environments*. Houston, Tex.